SFERA-III

Solar Facilities for the European Research Area

Improving concentrated solar ageing services

Deliverable D9.4

Estimated delivery date:	20.05.2021
Actual delivery date:	28.02.2023
Lead beneficiary:	CNRS
Person responsible:	Emmanuel Guillot
Deliverable type:	☒ R ☐ DEM ☐ DEC ☐ OTHER ☐ ETHICS ☐ ORDP
Dissemination level:	☒ PU ☐ CO ☐ EU-RES ☐ EU-CON ☐ EU-SEC

THIS PROJECT HAS RECEIVED FUNDING FROM THE EUROPEAN UNION'S HORIZON 2020 RESEARCH AND INNOVATION PROGRAMME UNDER GRANT AGREEMENT NO **823802**

AUTHORS

Author	Institution	E-mail
Audrey Soum-Glaude	CNRS	Audrey.Soum-Glaude@promes.cnrs.fr
Jean-Louis Sans	CNRS	Jean-louis.sans@promes.cnrs.fr
Emmanuel Guillot	CNRS	Emmanuel.Guillot@promes.cnrs.fr
Eneko Setien	CIEMAT	Eneko.Setien@psa.es
Loreto Valenzuela	CIEMAT	Loreto.Valenzuela@psa.es
Inmaculada Cañadas	CIEMAT	i.canadas@psa.es

DOCUMENT HISTORY

Version	Date	Change
v1.0	22.12.2021	Initial release
v2.0	28.02.2023	Revised version

VALIDATION

Reviewers		Validation date
Emmanuel Guillot	Emmanuel.Guillot@promes.cnrs.fr	22.12.2021
Ricardo Sanchez	Ricardo.Sanchez@psa.es	08.01.2022

DISTRIBUTION LIST

Date	Recipients
28.02.2023	SFERA-III WP leaders

Disclaimer

Executive Summary

Worckpackage 9 from the SFERA-III project focuses on improving services to develop and test high performance solar receiver. This includes in-situ thermo-mechanical assesment (task 1), better temperature measurements (task 2 and 3), and improved aging services (task 4).

Accelerated aging of solar receiver materials are provided at CNRS by the SAAF service at MSSF, and at CIEMAT at the solar dish facilities and at the SF60 solar furnace. The services (exceot the latter) were developed in SFERA-I and already enhanced with other projects such as SFERA-II and RAISELIFE. Further upgrades are required to comply with the user major requests and are being carried out under the SFERA-III project.

The ageing services upgrades were the following:

- CNRS **improved the temperature instrumentation and developed a new sample holder** for the SAAF service to answer the requests especially from the absorber coatings developers who use round samples which could not be tested previously.
- CIEMAT commissioned a new test bench at solar furnace SF60 for **ageing of tubular samples and assessing mechanical stresses**.

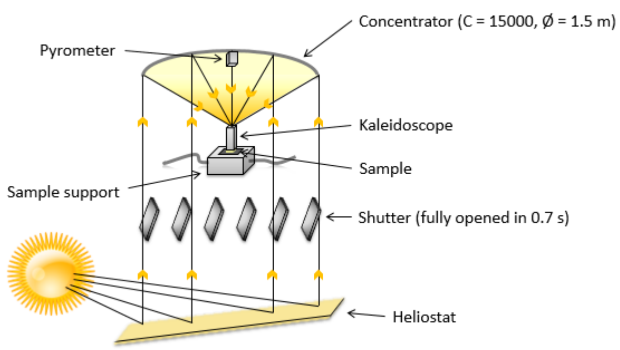

Closely related to this topic, the reader is also invited to refer to other SFERA-III publications from WP9, especially about emissivity measurements (including Deliverable 9.3 and milestone report MS26) and flux measurements (WS5 report), that have been or will be published during the project.

Table of Contents

Table of Figures

List of abbreviations

CSP	Concentrated Solar Power
IR	Infrared : beyond 800 nm
NIR	Near Infrared (typically : about 800 to 1700 nm)
O.D.	Outer diameter
PROMES	Laboratory for PROcesses, Materials and Solar Energy (CNRS)
PSA	Plateforma Solar de Almeria (CIEMAT)
SAAF	Solar Accelerated Aging Facility (CNRS)
SSAC	Solar Selective Absorber Coating
TC	Thermocouple
UV	Ultra Violet: below 400 nm

1. Improvement of CNRS Solar Accelerated Aging Facility (SAAF)

1.1. SAAF description and limitations

The Solar Accelerated Aging Facility (SAAF) installed at PROMES-CNRS laboratory in Odeillo allows applying constant or cyclic concentrated solar fluxes on samples to test their aging behavior and durability (Figure 1).

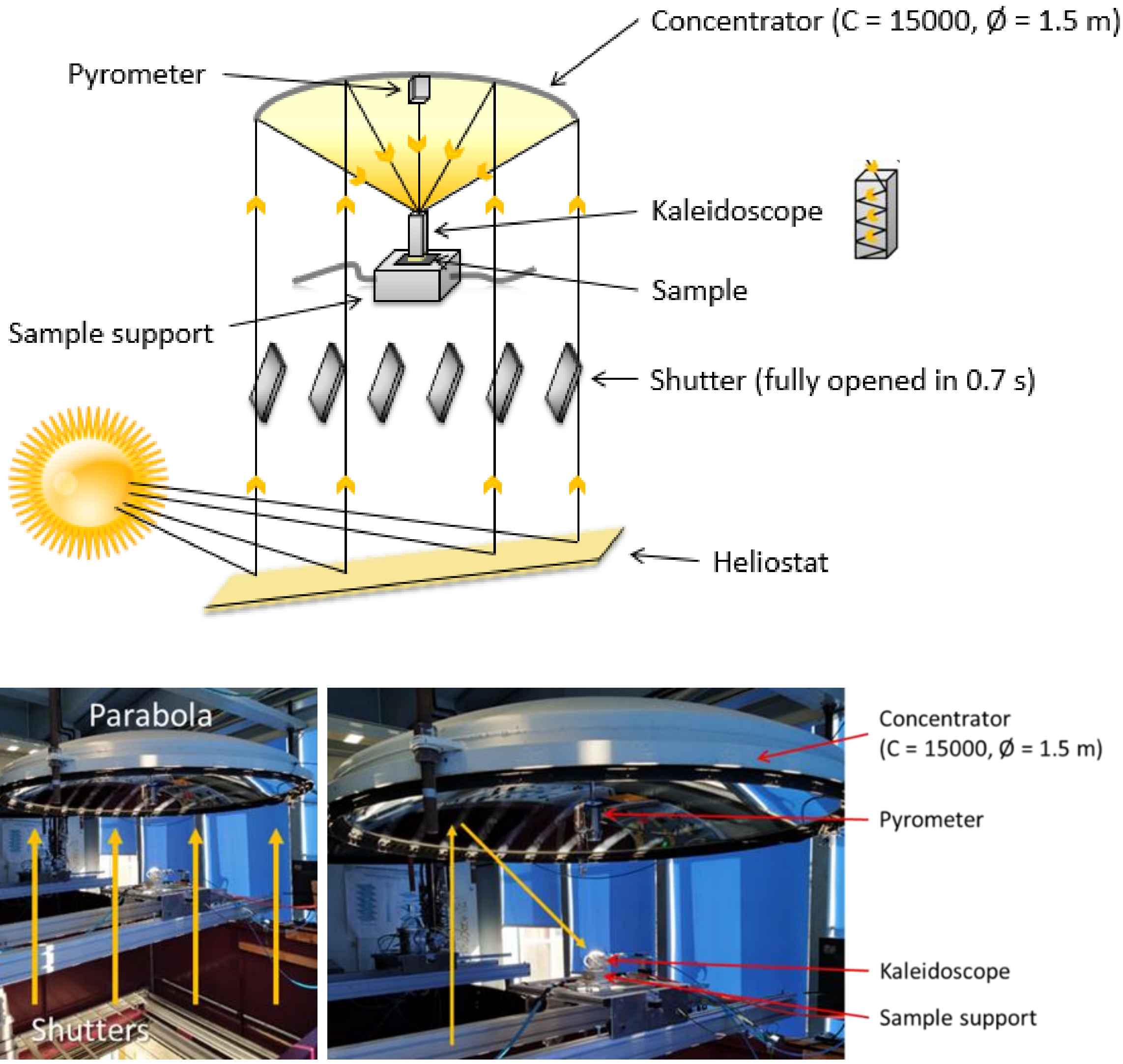

Figure 1. Solar Accelerated Aging Facility (SAAF)

SAAF consists in the following elements:

- a movable heliostat (20 m^2), installed on the first floor of the building, tracks the Sun and reflects parallel beams of solar irradiance toward the sixth floor, through a trap door equipped with controllable shutters to regulate the solar irradiance sent inside the building;
- a 1.5 m fixed parabolic dish concentrator, suspended horizontally above the trap door and shutters, receives solar irradiance from the heliostat and concentrates it at its focal point;
- a kaleidoscope (made of four mirrors facing one another) at the focal point homogenizes the concentrated solar flux (from a Gaussian profile to a **rectangular profile of approx. 20 x 20 mm**);
- a **sample holder** mounted on a movable cart is placed after the kaleidoscope to irradiate samples with a homogenized concentrated solar irradiance, whose flux density is controlled via the shutters;
- a solar-blind **pyrometer** (4.6 – 5.4 µm) suspended to the parabola right above the sample holder measures the **sample surface temperature** during the tests;
- a data acquisition system including a Graphtec data logger records input and output data (temperatures, voltages, flows, etc.).

SAAF was initially developed to test the solar and thermal performance of 50 x 50 mm^2 samples of high temperature (up to 1200°C), highly absorptive and highly emissive absorber paint coatings for CSP tower receivers (Pyromark®-coated Inconel samples, Figure 2) [1–4]. Sample surface temperature was regulated by backside air cooling and followed by front side solar-blind pyrometry through the illuminated area.

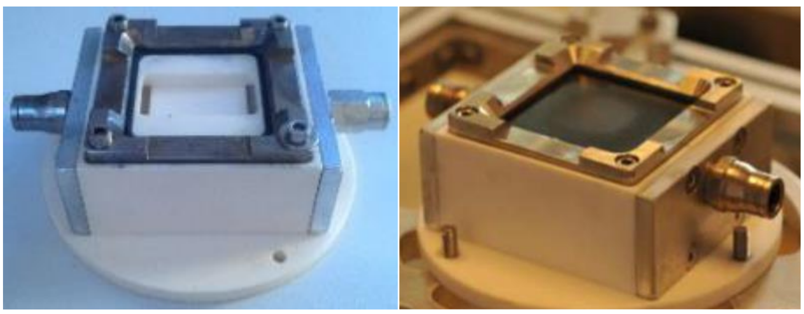

Figure 2. Initial SAAF sample holder (left), mounted with Pyromark®-coated Inconel sample (right)

In later studies, SAAF was used to test samples of **solar selective absorber coatings**

(SSACs) on metallic substrates provided by various coating developers. These complex coatings are designed and optimized to provide high optical performance for solar receiver surfaces, based on their spectral selectivity, i.e., high solar absorptance (α_S > 90%) in the solar spectrum (UV-Vis-NIR spectral range), combined with low thermal emittance (ε(500°C) < 15-20%) to reduce radiative thermal losses at high temperature (IR spectral range). The assessment of their aging behavior and resistance when submitted to concentrated solar irradiation is critical, as these conditions are close to working conditions in CSP technologies.

These new types of samples are not well adapted to the initial SAAF configuration:

1. SSACs samples have **various shapes and dimensions**, imposed by the manufacturer coating deposition facilities. For instance, sample substrates are often round as they are cut from round bars, easier to machine than square ones. Therefore, some samples cannot be maintained in the initial square sample holder, which requires samples of at least 2” in diameter (Figure 3). Also, temperature regulation by backside air cooling during the tests is not always possible or efficient due to the lack of airtightness (Figure 3).

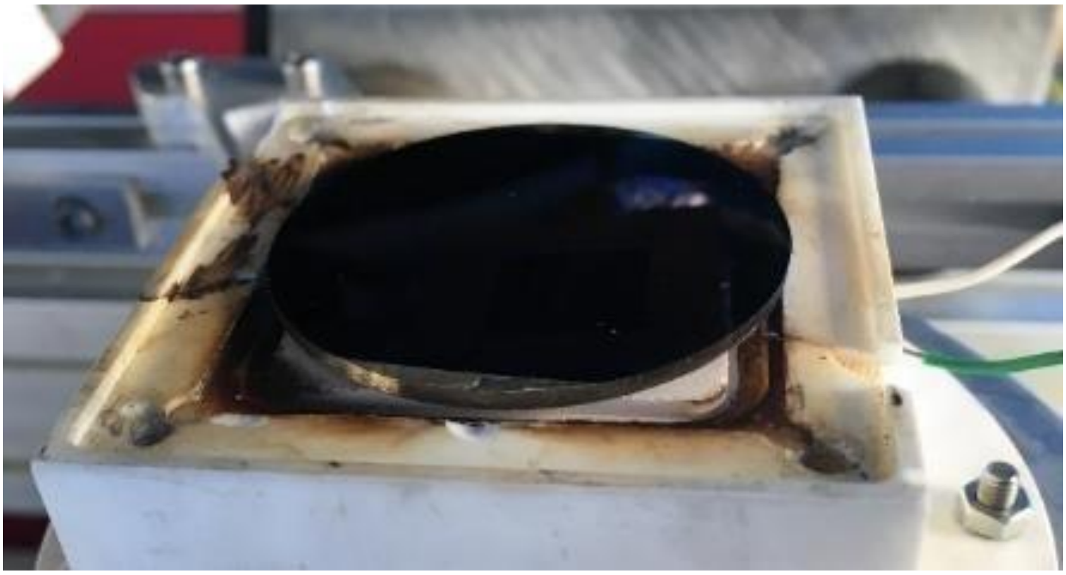

Figure 3. Initial SAAF sample holder (square) mounted with a sample of solar selective absorber coating deposited on Inconel (round)

2. the loss of the SSACs spectral selectivity can strongly reduce the overall performance of solar receivers, therefore it is critical to follow their spectral

optical properties after each aging step. This is rendered difficult by the size requirements of the initial sample holder, where the irradiated area of 20 x 20 mm² is located at the center of the 2" samples (Figure 4 (a)). Indeed, the IR spectrophotometer used in PROMES-CNRS laboratory (SOC100-HDR + Nicolet 6700 FTIR) to assess thermal emittance cannot measure the irradiated area of the O.D. 2" samples (area 2 in Figure 4 (c)): due to hindrance constraints with the IR source, it can only measure the side of the sample (area 1). Alternately, the sample can be cut to measure the irradiated area (Figure 4 (b)) but then aging tests are no longer applicable, which is not desirable. Smaller sample sizes are thus needed to follow the evolution of thermal emittance with aging, typically O.D. 30 mm. These smaller sizes are also preferable for other typical material characterization techniques.

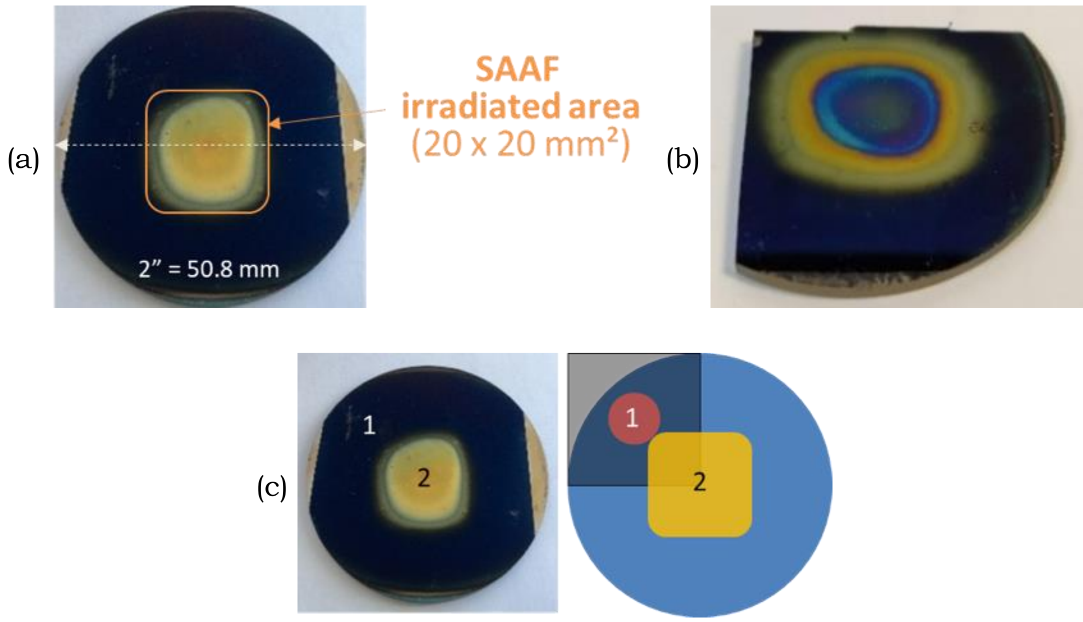

Figure 4. Sample area irradiated by SAAF (2); measured with PROMES-CNRS IR spectrophotometer (1)

3. the by-design low infrared thermal emittance of SSACs, and their lower thermal stability imposing lower testing temperatures (typically < 600°C), provide low signal-to-noise ratio for the detection of their luminance, and the measurement of their temperature by front side **pyrometry** in the 4.6 - 5.4 µm range is **less reliable**, even impossible at mid-temperatures. Also, pyrometry relies on the knowledge of the sample spectral emittance, to be measured prior to the aging tests, and can evolve during the latter giving rise to faulty temperature

measurements.

These limitations to the study of SSACs samples (or other low-emissive material) solar aging behavior in SAAF facility were addressed, as explained in the following sections.

1.2. Sample holder adaptation

To address limitations 1 and 2, a new sample holder was designed in PROMES-CNRS by Roger Garcia, fabricated and tested in SAAF (Figure 5). The primary objectives of this new sample support are to allow the treatment of samples of various shapes (round, square, rectangular) and sizes (typically 1" to 2"), while ensuring backside air cooling in all cases to better control/regulate the sample temperature.

This new support consists in:

1. a **static stainless steel structure**, integrating:
   - 1.1. **a gas inlet for backside compressed air cooling**. This air cooling system is less efficient than for the initial support, as the sample is not sealed to the support in this case, but it was found sufficient to limit the maximum temperature of the sample during aging tests below 600°C.
   - 1.2. a **feedthrough to insert a thermocouple** in contact with the back center of the sample, as an indication of the sample surface evolution, in complement to pyrometer front center temperature measurements. This point is further discussed in the next section.
2. **a hollow top cover** (header), to hold the sample while allowing it to be irradiated (central area of 20 x 20 mm^2). Only the edges of the sample are maintained by the cover in four points, and on its back side the sample is held by ceramic sticks inserted in the static structure, to limit conductive losses. Two concentric sets of three holes have been drilled into the static structure to insert these ceramic sticks.

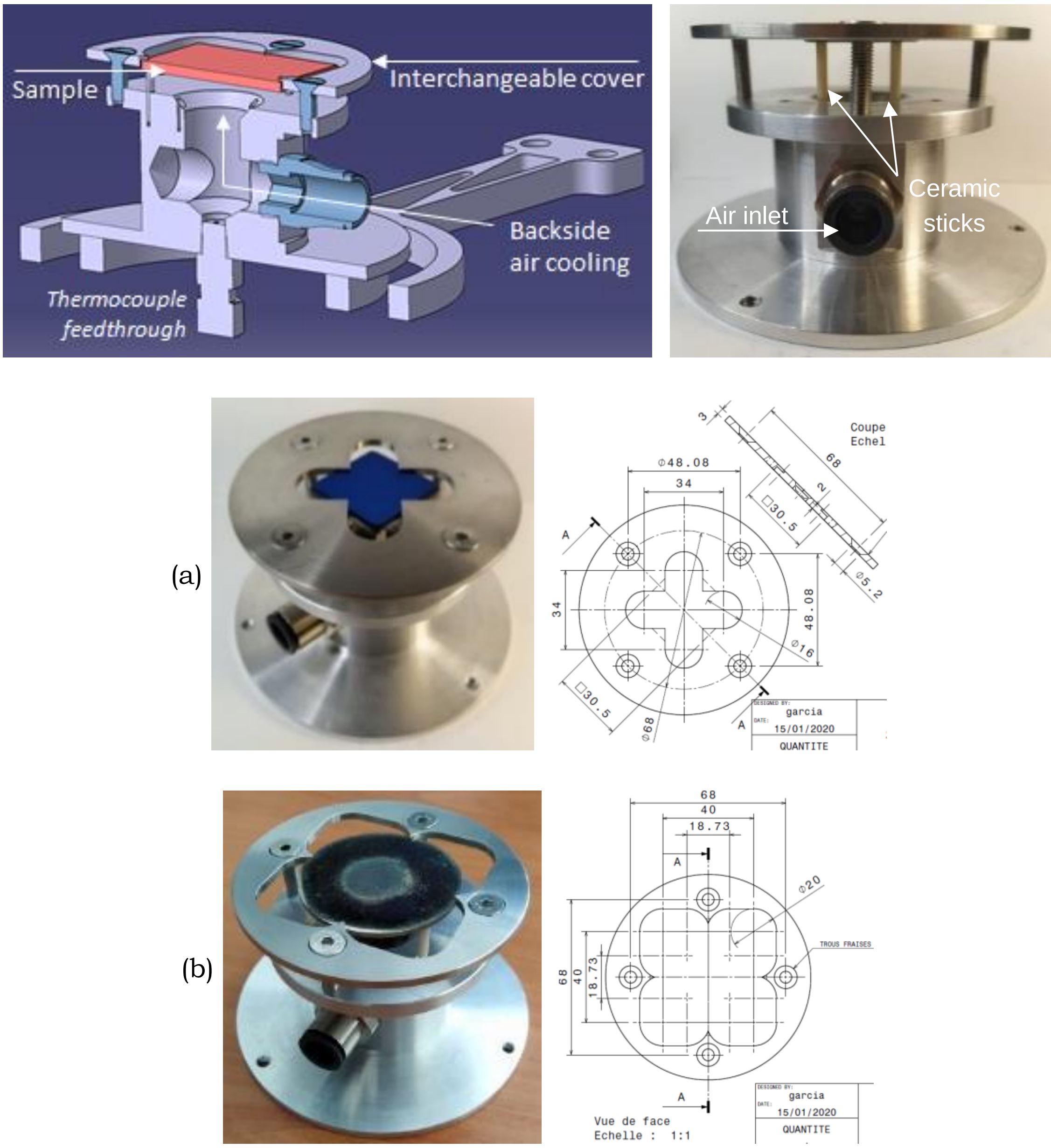

Figure 5. New SAAF sample holder

They are matched with two interchangeable covers, adapted to different sample dimensions:

2.1. one cover is for smaller samples (Figure 5 (a)), although with dimensions larger than the SAAF-irradiated area (20 x 20 mm²): for instance, samples that are round with diameter 1", or square or rectangular with dimensions 25 x 25 mm², or 25 x 30 mm², or 30 x 30 mm², or 33 x 33 mm², etc. have been successfully fitted in the sample holder using this cover.

2.2. the other cover is for larger samples (Figure 5 (b)): typically, round with diameter 2”, or square with dimensions 50 x 50 mm², etc. *N.B. These larger samples could also be tested using the smaller cover, but then a much larger area of the sample would be in contact with the metallic cover: conductive thermal losses would be increased, as well as mechanical constraints on the sample.*

If need be, additional covers can easily be designed and machined to adapt to other sample shapes and dimensions, within the limits imposed by the dimensions of the irradiated area (larger than 20 x 20 mm²) and the static structure (no larger than 50 x 50 mm²).

Due to its design, this sample holder also has a larger tolerance in sample thickness. As for the previous sample holder, a thickness of at least 2 mm is recommended to limit sample thermomechanical deformation due to high temperature aging tests.

This new sample holder has been commissioned in 2020, using various samples of solar selective absorbers, and is now available for SAAF users. Although it was initially developed for SSACs, it can also be used to expose any type of sample to concentrated solar constant or cyclic irradiation for accelerated aging purposes, typically below 600°C. Thermal aspects related to the new sample holder will be discussed in the following section.

1.3. Temperature instrumentation

New experiments and calculations were carried out regarding the temperature instrumentation, temperature levels and temperature profiles seen by the samples during solar exposure in SAAF, deepening the knowledge and control of this facility.

1.3.1. Pyrometry measurements

The sample surface temperature is measured using an OPTRIS G5H CF4 pyrometer (Figure 6). The detection of the sample thermal emission is carried out through the incident solar radiation in the kaleidoscope (see §1.1 p.8). The pyrometer has a spectral response between 4.8 and 5.2 µm (Figure 6, right), and is thus considered solar blind since solar irradiance occurs below 2.5 µm (> 99%). Therefore, pyrometry measurements are supposedly not perturbed by the incident solar irradiation. Due to its spectral range, the pyrometer only measures temperatures above 250°C.


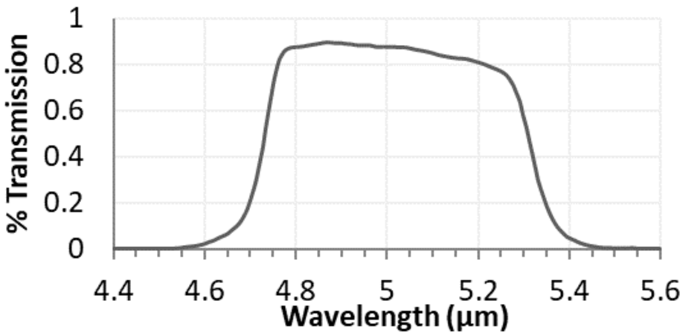

Figure 6. OPTRIS G5H CF4 pyrometer picture and spectral transmittance

1.3.1.1. Pyrometer calibration

First, the pyrometer was recalibrated in temperature using a blackbody SR-2 from ECI systems (Figure 7) with ε = 0.99 ± 0.01. The temperature of the blackbody was varied from 250 to 1150°C with a step of 50°C. Figure 8 shows the temperature read by the pyrometer with input emittance of 0.98 (maximum available value) (see Table 3 p. 44 for data). This calibration showed that the SAAF pyrometer gives accurate measurements, with maximum relative errors of ± 2-3%, when the emittance of the measured body is high (high signal-to-noise ratio).

Figure 7. Pyrometer calibration set-up

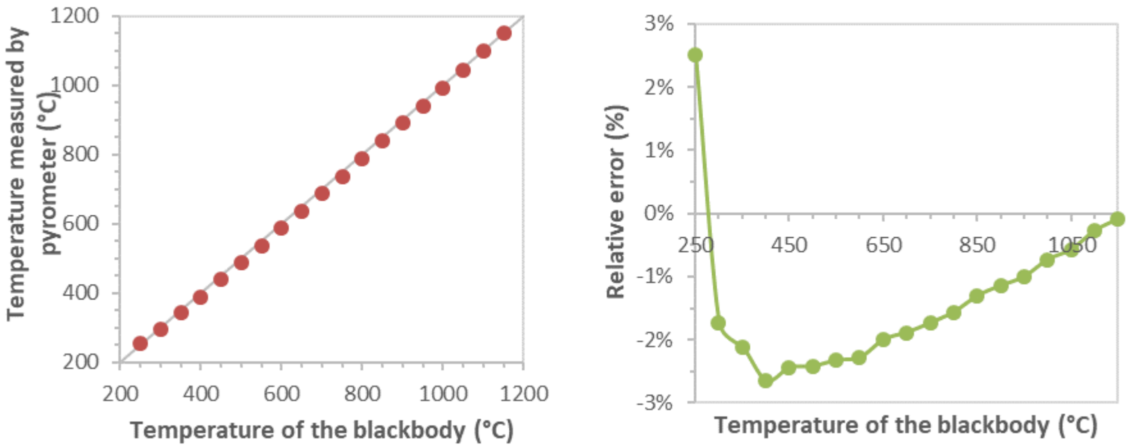

Figure 8. Temperature read by pyrometer vs. real blackbody temperature (left), relative error committed by pyrometer (right)

1.3.1.2. Propositions for a new pyrometer

The pyrometer model was initially chosen to measure sample temperatures well above 250°C and on highly emissive materials such as Pyromark® high temperature absorbing paint ($\varepsilon_{VIS\text{-}SWIR\text{-}MWIR} = 0.95$).

For the study of solar selective absorber coatings, it has been considered to replace the current pyrometer with a model more adapted to their by-design low IR emittance ($\varepsilon_{MIR} < 0.10$) and their lower thermal stability, that give rise to low signal-to-noise ratio and lower temperature measurement accuracy, compared to previous studies. To do so, there are several points to take into account.

1.3.1.2.1. Spectral range of the pyrometer

The typical solar spectrum in Odeillo has previously been calculated by C. Gueymard using SMARTS and Modtran software [5], based on typical atmospheric conditions at this location. From these simulations, it is observed that the Sun emits, apart from the classical spectral range between 280 and 2500 nm, a small amount of radiation in the mid-IR range (Figure 9). *N.B. As a comparison, the maximum spectral irradiance is 1.65 W/m²/nm, around 495 nm.*

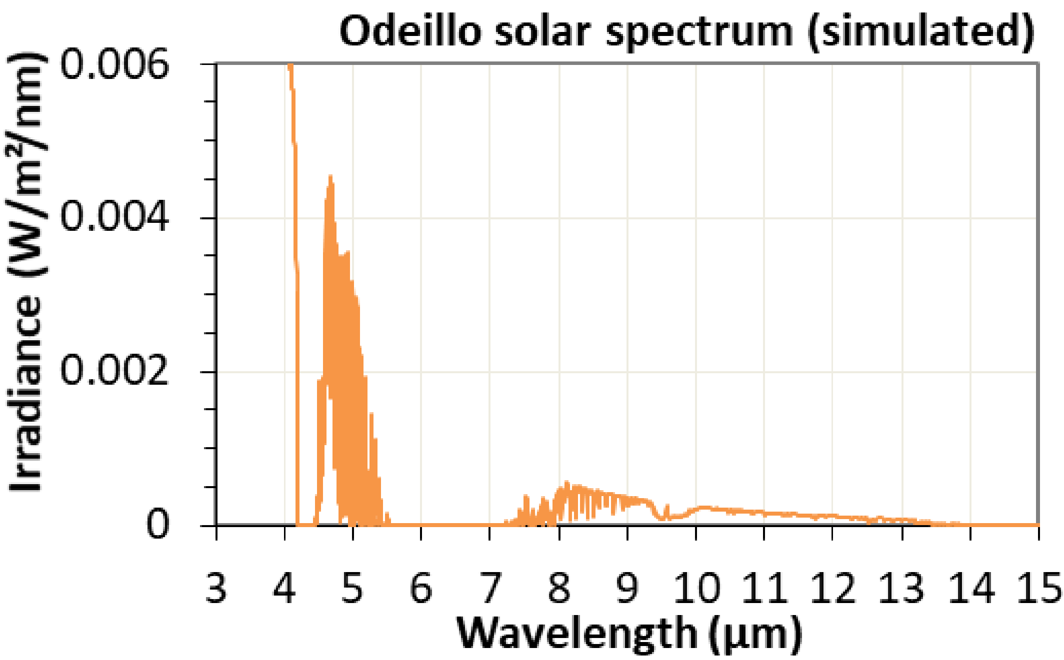

Figure 9. Solar spectrum in Odeillo simulated using SMARTS-Modtran, between 3 and 15 µm (C. Gueymard) [5]

This solar IR emission can be problematic for the use of a pyrometer in SAAF, where the sample emission measurement is done on the same surface as the one receiving the solar concentrated incident radiation. The sample can indeed reflect part of the incident solar radiation towards the pyrometer, which is added to the emission of the hot sample itself, causing the temperature estimation to be incorrect. This is particularly true for SSACs which are highly reflective in the IR range (much like metals) and even more so when the material temperature and subsequent radiative emission are low.

1.3.1.2.2. Signal-to-noise ratio

In order to estimate a "signal-to-noise" ratio, the solar reflection and thermal emission of the sample in different conditions have been estimated and compared, in typical pyrometer spectral ranges, so as to check if they are "solar blind" in said range. OPTRIS pyrometers have been considered as a reference (see Annex p.45). Parameters such as shutters opening (%) and sample temperature have also been varied.

A typical SSAC sample (SS/W/WAlSiN/SiON/SiO_2 [6]) was chosen as reference for calculation. Its measured spectral reflectance is shown in Figure 10.

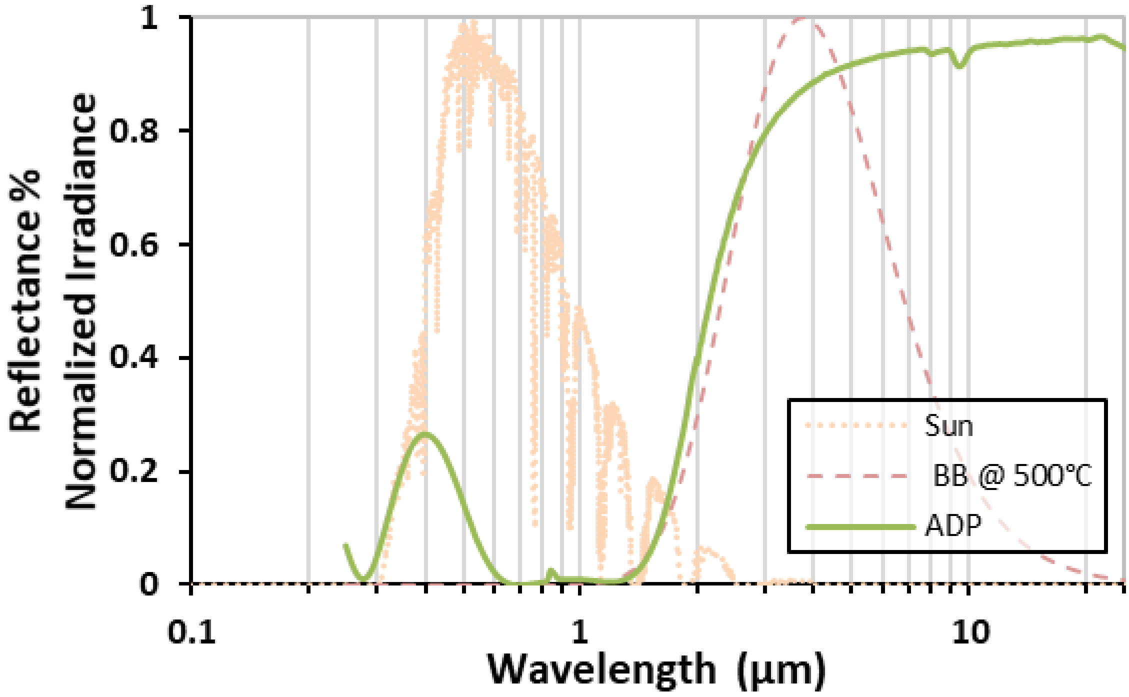

Figure 10. Spectral reflectance of SS/W/WAlSiN/SiON/SiO2 [6] SSAC sample with low solar reflection and high IR reflection (in green). As reference, the radiative sources for the sun (dotted orange) and a black body at 500°C (dashed purple).

The sample emitted flux density (i.e. the "signal", in W/m²) in different spectral ranges (λ_1, λ_2) and temperatures T was calculated by:

1. deducing its spectral emittance as 1 – spectral reflectance, measured by spectrophotometry (at room temperature, since reflectance is rather constant with T for these materials [7]) (Figure 16 11);
2. weighting it by the blackbody spectrum (i.e., Planck's law integrated over solid angle $P(\lambda,T)$, Equation 2) in said spectral range and temperature;
3. integrating this product over wavelength, to obtain the total emission of the sample at a given temperature, in W/m², in the spectral range of interest;
4. subtracting the radiative emission received from ambient, i.e., the blackbody spectrum at T_0 = 20°C integrated in said spectral range. As a comparison, the case without this contribution (i.e., for T_0 = -273.15°C) was also considered.

The procedure is summarized by Equation 1.

Equation 1 $$E_{tot}([\lambda_1,\lambda_2],T) = \int_{\lambda_1}^{\lambda_2}[1 - R(\lambda)] \cdot P(\lambda,T) \cdot d\lambda - \int_{\lambda_1}^{\lambda_2} P(\lambda,T_0) \cdot d\lambda$$

Equation 2 with $P(\lambda,T) = \frac{2\pi hc^2}{\lambda^5[e^{hc/(\lambda kT)}-1]}$

Concerning the solar flux density reflected by the sample (i.e., the "noise", or parasitic measurement), the one received by the sample was first estimated, in each spectral range of interest (λ_1, λ_2):

1. the Odeillo solar spectrum $G(\lambda)$ (Figure 9) was used as a reference;

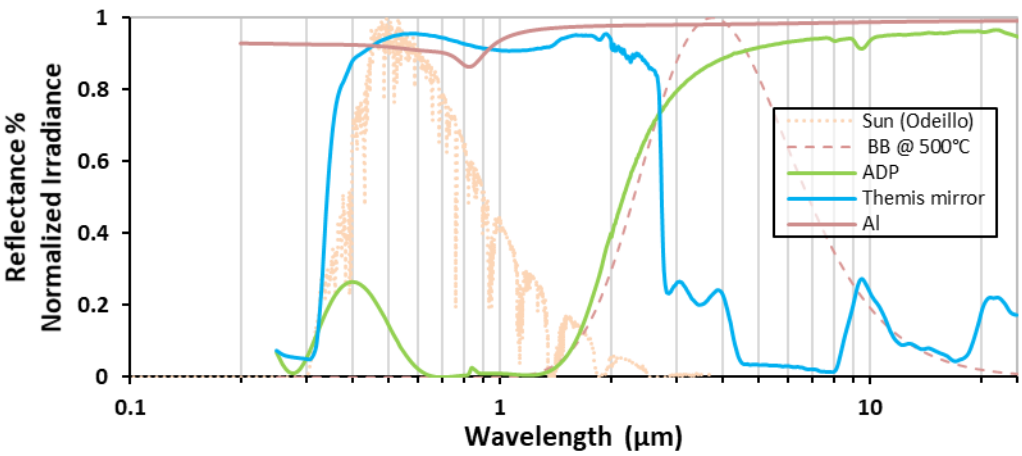

Figure 11. Reflectance spectra of Themis heliostats (blue, C. Escape / C. Caliot), Al mirror (red), as-deposited sample (green) As reference, the radiative sources for the sun (dotted orange) and a black body at 500°C (dashed purple).

2. to take into account the different stages of reflections from the mirrors, this solar spectrum was multiplied by the reflectance spectra from the heliostat and the parabola (both being silver reflectors below thick glass), and the kaleidoscope mirrors (aluminum-coated steel). The first two spectra were represented by the one previously measured at PROMES-CNRS on Themis heliostats (Figure 11), as these mirrors are of the same nature. The last one was approximated by the reflectance spectrum of pure Al, calculated from Al optical indices found in the literature [8], using classical optical theory [9] (Figure 11). This tends to overestimate the reflectance of the kaleidoscope

mirrors, and thus the solar radiation actually received by the sample;

3. this modified incident solar spectrum was then multiplied by the sample spectral reflectance (Figure 16);
4. the resulting spectrum was integrated over the spectral range of interest, to estimate the solar flux density reflected by the sample towards the pyrometer, in W/m² (Equation 3);
5. to take into account the concentration of this solar radiation by the parabola, a relative concentration ratio *C* was deduced from calorimetry measurements done on SAAF on March 10, 2017 (H. Thibault, F. Lecat). The latter gave an estimation of the concentrated solar flux density obtained after the kaleidoscope (see Figure 1 p.8), as a function of the shutter opening, for a DNI of 1000 W/m², for the whole spectrum (Figure 12). Values of *C* vs. shutters opening were thus deduced using the usual definition of 1 sun = 1000 W/m² (Table 1);

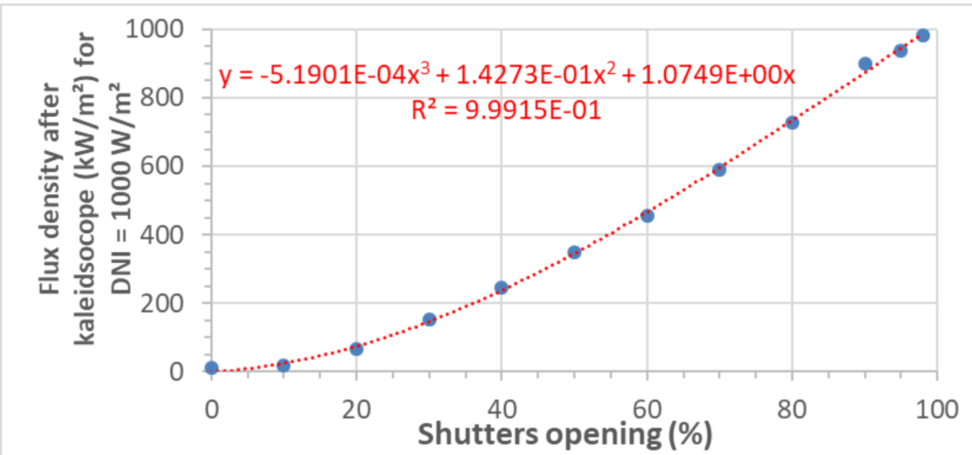

Figure 12. Concentrated solar flux density after SAAF kaleidoscope vs. shutters opening (%) for an incident solar flux density of 1000 W/m²

Table 1. **Estimated relative concentration ratio and transfer function *F* vs. shutters opening.**

% opening	0	10	16	20	24	30	36	40	41	46	50	60	70	80	90	100
C or	0	25	52	74	101	147	199	238	248	301	346	466	597	734	874	1016

Table 1. **Estimated relative concentration ratio and transfer function *F* vs. shutters opening.**

kW/m²																
F	0	32	67	97	132	192	261	311	324	393	452	609	780	959	1143	1328

6. so as not to take into account twice the reduction of solar input due to the imperfect mirror solar reflectance, which is already considered in the modified solar spectrum, these values of C were divided by the solar reflectance R_S of all involved mirrors (two silver ones for the heliostat and parabola, an aluminium one for the kaleidoscope), to approximate a "transfer function" F of the system (Equation 4, Table 1). R_S values were calculated for each type of mirror, by integrating the mirrors spectral reflectances over the whole Odeillo solar spectrum (Equation 5): R_S (Ag) = 0.9099944, R_S (Al) = 0.9238001;
7. finally, the above reflected solar flux density was multiplied by F (Equation 3).

Equation 3
$$R_{tot}([\lambda_1, \lambda_2]) = F \cdot \int_{\lambda_1}^{\lambda_2} G(\lambda) \cdot R_{Ag}^2(\lambda) \cdot R_{Al}(\lambda) \cdot R_{sample}(\lambda) \cdot d\lambda$$

Equation 4
$$C = R_S^2(Ag) \cdot R_S(Al) \cdot F$$

Equation 5
$$R_S = \frac{\int_{0.28\ \mu m}^{16.13\ \mu m} R_{mirror}(\lambda) \cdot G(\lambda) \cdot d\lambda}{\int_{0.28\ \mu m}^{16.13\ \mu m} G(\lambda) \cdot d\lambda}$$

Several cases of shutters opening and temperatures were calculated (using a Scilab specially developed code), considering four OPTRIS pyrometers (2ML, G5, P7, LT) with relevant temperature and spectral ranges (see Annex 2 p.45). As an example, shutter openings of 20%, 40% and 60%, and temperatures from 100°C to 400°C were considered: corresponding data is gathered in Table 2.

Table 2. **Calculated solar reflected and emitted flux densities of a typical SSAC sample**

Spectral range	**OPTRIS pyrometer**		**Solar flux density (W/m²)**				**Emitted flux density (W/m²) at temperature *T, hemispherical***			
	Model	***Temp. detection range***	***Odeillo 1.15AM best***	***Reflected by sample (shutters 20%) C ≈ 74***	***Reflected by sample (shutters 40%) C ≈ 238***	***Reflected by sample (shutters 60%) C ≈ 466***	***100°C***	***200°C***	***300°C***	***400°C***
1.5 - 1.7 µm	2ML	250 - 800°C	47.82	403	1289	2524	0.0003 *0.0003*	0.04 *0.04*	1.03 *1.03*	10.34 *10.34*
4.6 - 5.4 µm	G5	100 - 1650°C	1.39	0.14	0.44	0.86	3.54 *-1.74*	18.11 *12.83*	52.74 *47.46*	112.45 *107.17*
7.5 - 8.5 µm	P7	0 - 710°C	0.27	0.06	0.18	0.36	5.58 *-19.11*	15.68 *-9.01*	31.15 *6.46*	51.08 *26.39*
8 - 14 µm	LT	-50 - 1030°C	1.04	2.52	8.07	15.79	24.45 *-130.66*	56.52 *-98.59*	99.91 *-55.20*	151.85 *-3.26*

For the emitted flux density, the value in italics is calculated for ambient at 20°C, the other for -273.1°C = 0 K.

N.B. Shutters opening and temperature are correlated via the concentrated radiation received by the sample. The temperature profile obtained on the sample with a thermocouple on the back side indicates that at 50 kW/m² the sample is around 275°C and at 100 kW/m² it is at 375°C. In that case, the shutters opening would be around 16 and 24% respectively, so only the case at 20% opening can be considered and compared to the emitted flux density.

From these calculations, the signal-to-noise ratio corresponding to the sample can be deduced for the four models of OPTRIS pyrometers (Figure 13).

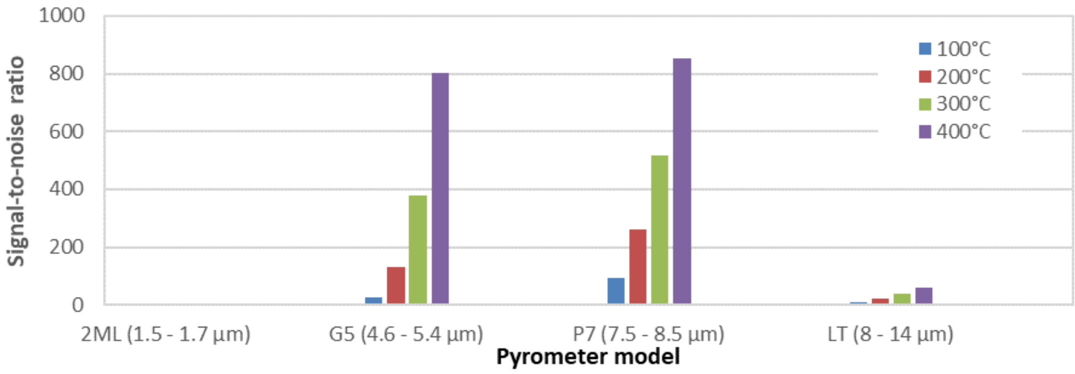

Figure 13. Estimated signal-to-noise ratio obtained for a typical SSAC during SAAF exposure (shutters open at 20%) at different low-mid temperatures, considering different OPTRIS pyrometer models

G5 model (4.6 – 5.4 µm, 100 - 1650°C) is the current pyrometer used in SAAF. Figure 13 shows that the P7 model (7.5 – 8.5 µm, 0 - 710°C) could be a more adapted solution for SSACs coatings at low-mid temperatures, with higher expected signal-to-noise ratios in the 100-400°C range, despite the noise due to the solar emission in the 7 – 9 µm range (Figure 9) that is concentrated then reflected by the SSAC sample with high IR reflectance (Figure 10). As a matter of fact, the parasitic reflection is even higher in the 4 – 6 µm range (Figure 9). Also, at these lower temperatures, the radiative emission of the sample is shifted towards higher wavelengths (cf. Wien's displacement law) and is thus better detected with a pyrometer having a higher wavelength range.

Apart from the P7 model, the other considered models are less performing than the current G5 model: at lower wavelength (2ML model, 250 - 800°C, 1.5 – 1.7 µm) the pyrometer is no longer solar blind and the noise is very high, and at higher wavelength (LT model, -50 - 1030°C, 8 – 14 µm) the emission from the sample becomes too low in the temperature range of interest compared to ambient noise.

Thus overall, the G5 model remains an acceptable choice, even when considering low-emissive low-temperature samples. Also, it allows better detection at temperatures higher than 400°C because of its spectral range covering lower wavelengths.

1.3.2. Thermocouple measurements

As a complement to pyrometry, and sometimes in substitution, especially at lower temperatures where the signal emitted by the sample is low (< 300°C), the sample was instrumented with thermocouples (TC) to follow its temperature at different positions. An advantage of this method is that with thermocouples, there is no need to know and measure the sample spectral emittance, whereas it is a mandatory input for pyrometry measurements.

1.3.2.1. Initial sample holder (configuration without backside cooling)

When using round 2" samples on the initial 50 x 50 mm² square sample holder, airtightness was not ensured and backside air cooling was not possible. However, it allowed for the instrumentation of the sample with K-type thermocouples (Figure 14).

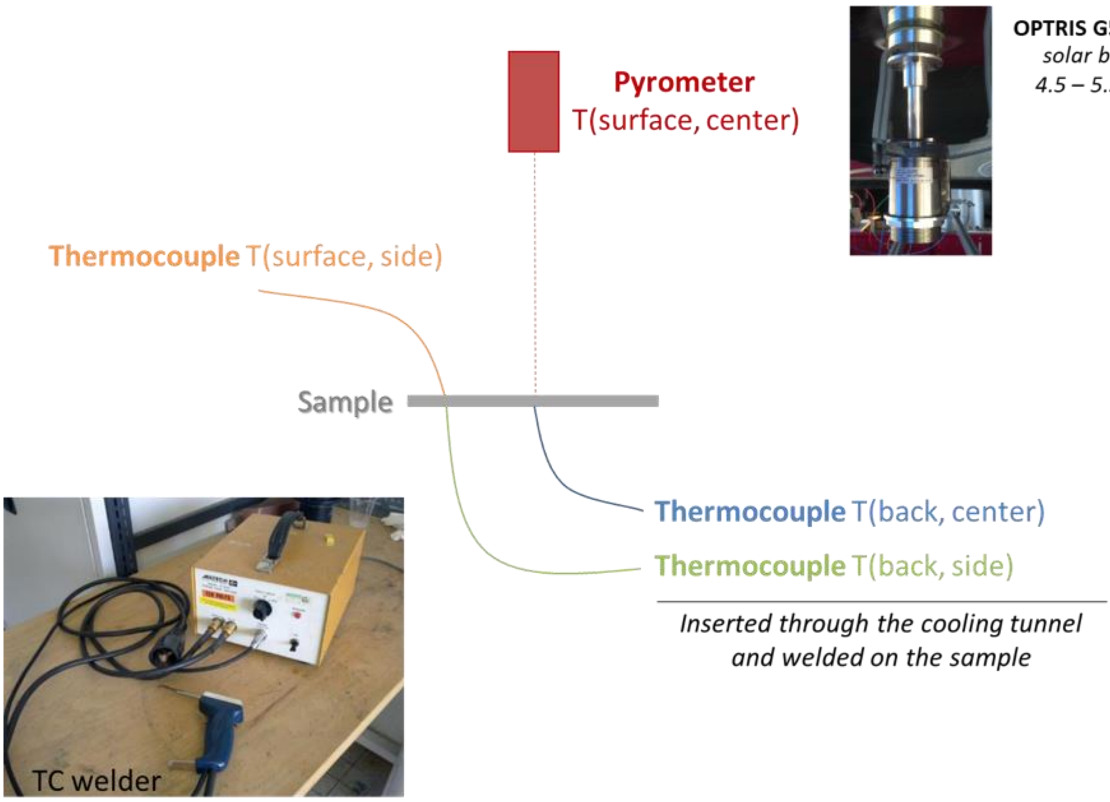

Figure 14. Sample temperature instrumentation

A thermocouple was welded on its backside center (blue), directly below the SAAF-irradiated area (see Figure 3, p. 10). Two thermocouples were also welded on the side of the sample, one above (orange in Figure 15), one below (green in Figure 15). Temperature was also measured with the pyrometer as a comparison (red). Temperature profiles were recorded using a Graphtec data logger and are reported in Figure 15.

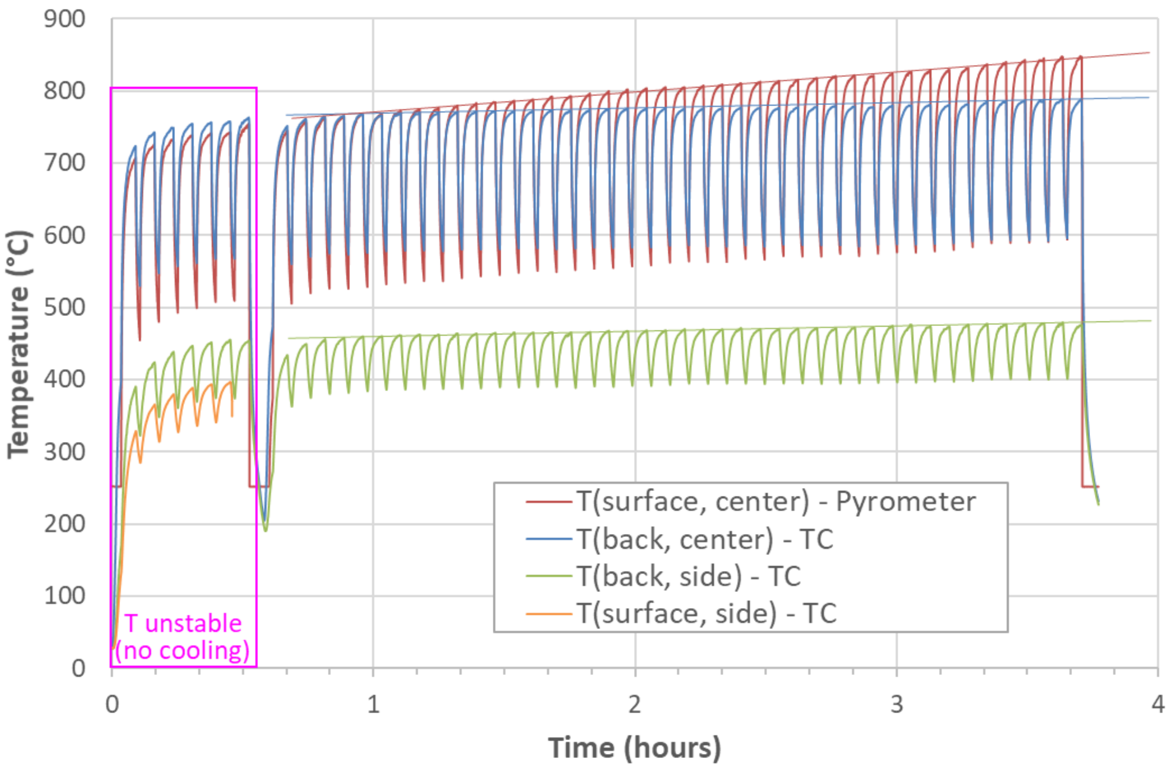

Figure 15. Sample temperature profiles

Overall, the back center thermocouple measurement (blue) is consistent with that of the pyrometer on the surface center (red), and is thus considered representative of the sample surface temperature. This conclusion is strongly comforted by many other similar measurements on various samples at different temperature levels [10].

The temperature measured on the sides of the sample (orange and green) is much lower, indicating high thermal gradients in the sample, due to its non-uniform solar exposure. However, there is a correlation between the temperatures measured on the side and the back of the sample, so that the temperature measured on the side could be used as an indicator of the sample temperature under exposure, depending on the substrate nature (thermal conductivity) and thickness.

The temperature measured with the pyrometer slowly increases with time. The ones measured with the TCs also increase but to a much lower extent. Therefore, it is possible that the sample emittance evolves during SAAF exposure, due to its aging. This begs the question of the validity of the temperature measured with the pyrometer, if the sample is aging during SAAF exposure.

In this regard, pyrometry is not the best option, and TCs are more reliable. However, the sample systematic instrumentation with welded TCs before each SAAF exposure is heavy to implement, especially since they must be removed after exposure for sample characterization. Also, TC positioning is not perfectly repeatable and may also introduce uncertainties. If the sample is maintained below its critical temperature (at which it suffers catastrophic changes), pyrometry may remain reliable.

1.3.2.2. New sample holder (with backside cooling)

As explained in section 1.2 (p.12), the new SAAF sample holder is equipped with a feedthrough to lay a thermocouple (O.D. 1.5 mm) in direct contact with the center backside of the sample. Such thermocouple (TC) measurement can be used as a complement or replacement for pyrometry measurements on the front side of the sample. The TC feedthrough also avoids having to weld the thermocouple to the sample backside before each measurement.

As a comparison, Figure 16 shows temperature measurements acquired by three methods during SAAF solar exposure, and compared: (1) a thermocouple was inserted in the feedthrough ("TC back center touching" in orange), (2) another thermocouple was welded on the back center of the sample near the previous one ("TC back center welded" in blue), and (3) a pyrometer measured the sample front center side (in red).

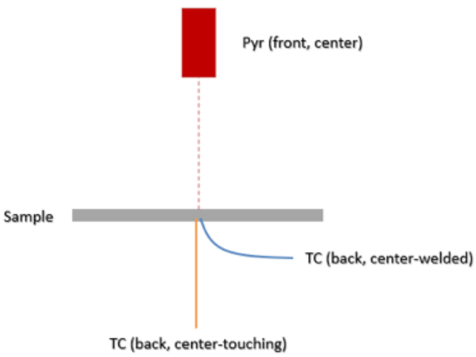

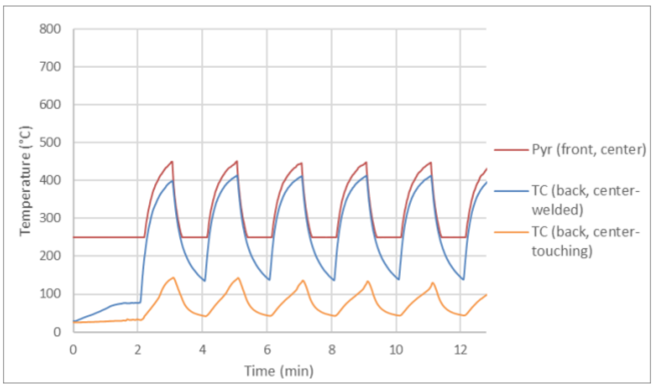

Figure 16. Schematics of sample temperature measurements with SAAF for the new sample support (left) and corresponding temperature profiles (right)

The welded TC measurement (blue) is overall consistent with that of the pyrometer (red) and is thus considered as representative of the sample surface temperature. *N.B. This tendency was even better confirmed in other cases where the TC was welded directly below the center of the irradiated area.*

Conversely, measurements by the thermocouple touching the backside of the sample (orange) only give a qualitative profile of the temperature variations, as they underestimate the sample temperature by several hundreds of °C. Indeed, as the flexible thermocouple (O.D. 1.5 mm) is simply "squashed" on the sample surface and not welded, there is a large thermal resistance between the TC and the sample.

However, the positioning and contact of the touching TC is more repeatable thanks to the maintaining feedthrough, compared to a welded TC. Therefore, a mathematical correlation could be found between touching TC and pyrometer measurements, depending on the nature (thermal conductivity) and thickness of the sample substrate (Figure 17). This correlation can be used for the prediction of the real temperature profile when pyrometry measurements are not reliable.

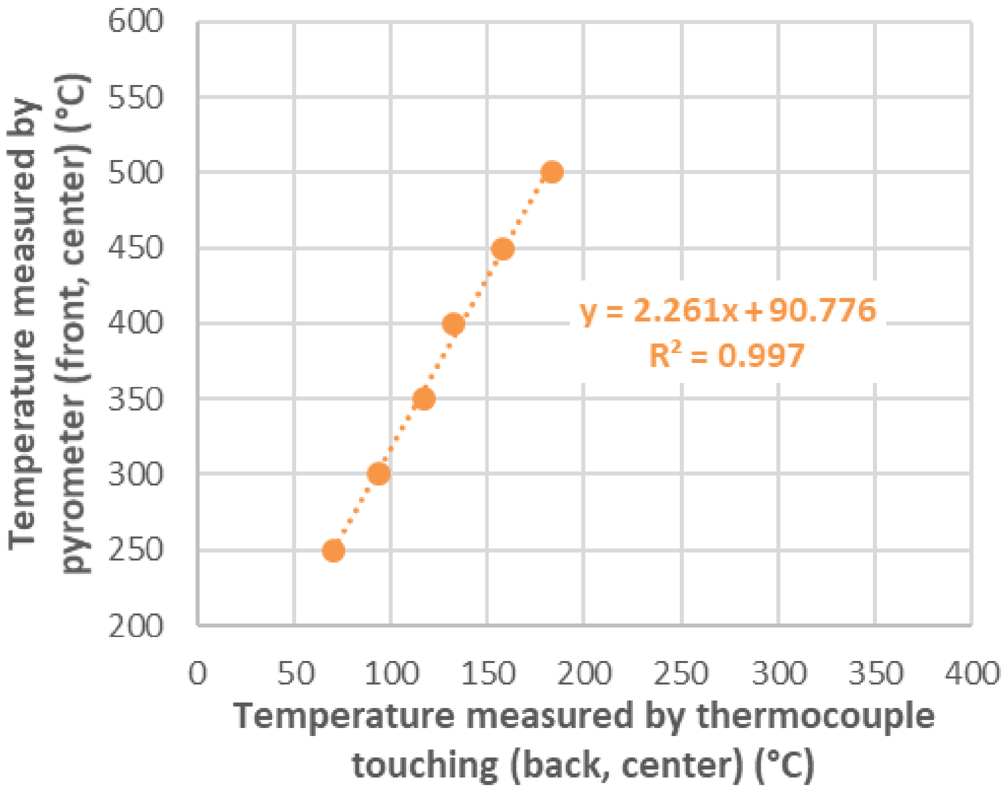

Figure 17. Correlation between temperatures measured by the pyrometer (center, front) and by the thermocouple touching (center, back) an Inconel-SSAC sample

1.3.3. Complementary data related to temperature levels in SAAF

Finally, new experiments with SSAC samples allowed SAAF temperature levels to be further evaluated. In particulier, sample heating and cooling rates, as well as temperature gradients within the sample, were measured.

1.3.3.1. Heating and cooling rates in SAAF

Figure 18 shows an example of heating/cooling profile recorded during SAAF cycling test on the surface center (pyrometer) and back center (welded thermocouple) of a 2 mm-thick Inconel sample with selective absorber coating. The thermal gradient (in °C/s) gives an image of the heating and cooling rates seen by the sample. The initial heating rate starting from room temperature is around 5°C/s, then between 15 and 25°C/s during the cycles. In this example, backside air cooling with gas flow around

0.0025 g/s was applied to the sample to control its temperature: this “regulated” cooling rate was ranging from -12 to -10°C/s. For the last cooling phase, the air cooling is stopped and the sample is allowed to cool naturally: its natural cooling rate reached around -20°C/s.

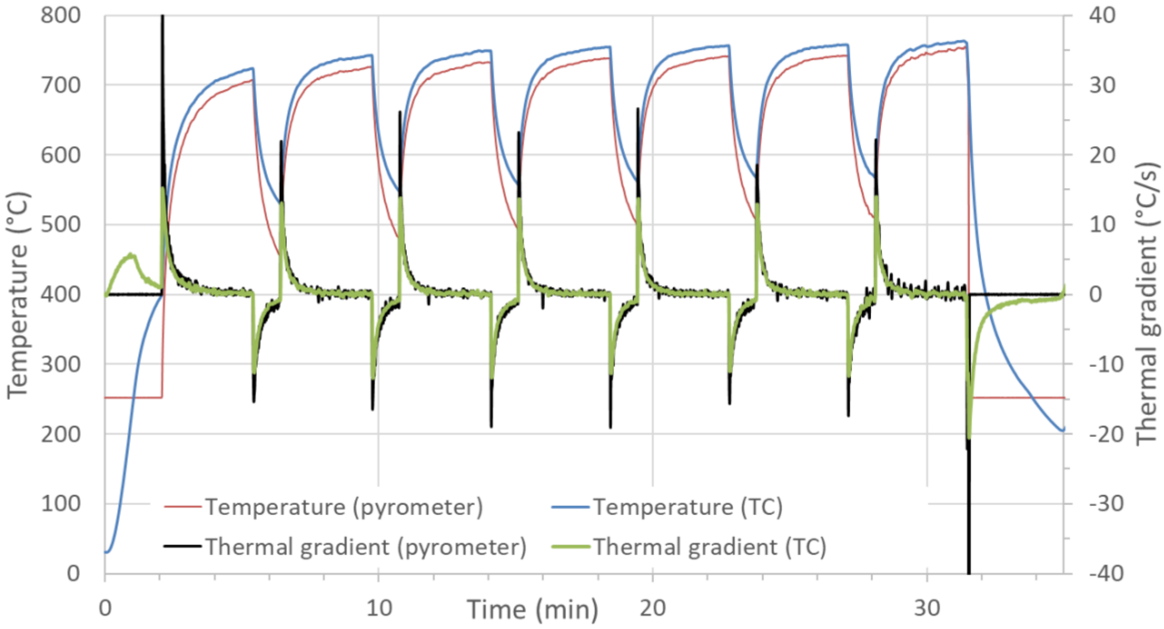

Figure 18. Example of heating/cooling profile obtained with SAAF on 2-mm-thick Inconel/SSAC sample

Heating and cooling rates may vary with the sample thickness and the air-cooling flow rate, if any. However, this example gives an order of magnitude of heating and cooling rate levels available with SAAF. Overall, they are much higher than would be attainable with an electrical furnace (typically 20°C/min), allowing for thermal shocks and rapid thermal cycling that are only accessible with such a set-up.

1.3.3.2. Temperature gradient in the sample during SAAF exposure

In SAAF, the irradiated samples can suffer a thermal gradient. Such high temperature gradients applied to a coating can be very damaging in themselves, especially at high temperature, as they generate high local thermomechanical stress.

For a better knowledge of the SAAF, these gradients were measured experimentally. The temperature distribution seen by an Inconel sample (diameter 50.8 mm, thickness 2 mm) during SAAF treatment (similar configuration as in Figure 3, p.10) was measured, using five thermocouples welded below the sample from its center to its side (Figure 19, right).

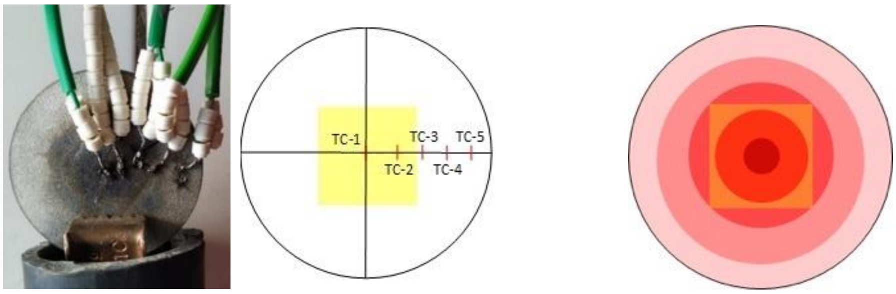

Figure 19. Positions of thermocouples welded on the back of the sample (left), estimated temperature distribution considering a radial symmetry (right)

TC-1 is located at the center and TC-2 to TC-5 are respectively at 6.5 mm, 11.5 mm, 16.5 mm and 21.5 mm from the center. The irradiated area is ±10 mm from the center (yellow in Figure 19).

The temperature distribution was reconstructed from these measurements (Figure 20, next page), considering a radial symmetry (Figure 19, right). While temperature is rather homogeneous (± 20°C) in the center of the irradiated area (in yellow), there is a quick drop in temperature on its sides, creating a high temperature gradient of -270°C between the center (0 mm, irradiated) and the edge of the sample (21.5 mm, not irradiated).

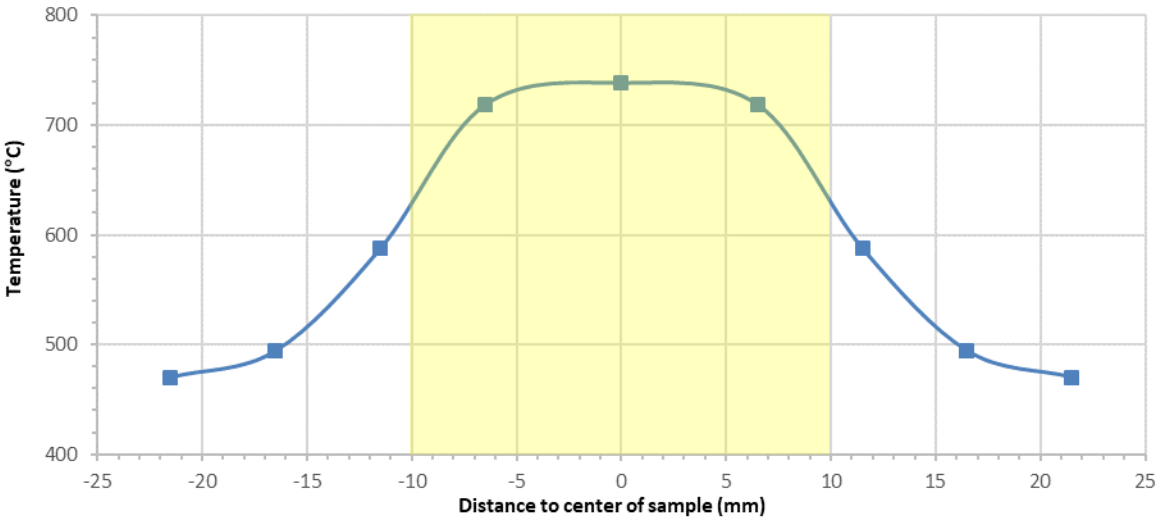

Figure 20. Temperature distribution measured on a SAAF-irradiated sample

1.3.4. Solar-blind pyroreflectometry

Pyroreflectometry is an active temperature measurement technique that use an active light source to assess the reflectivity of the sample. By combining in the same instrument a pyrometer and a reflectometer, under assumptions such as opaque sample, one can determine the true temperature of the sample without prior knowledge of its properties[11][12].

This technique is at a confidential commercial level due to its high complexity, but is developed and used at PROMES-CNRS for different setups such as MEDIASE for emissivity measurements at the big solar furnace using prototype instruments.

In the framework of SFERA-III, a first investigation has been conducted to check if this technique could be brought to the ageing services. The existing pyroreflectometers were deemed unsuitable as using wavelengths 1.3 and 1.5 µm, which are not solarblind and lead to unusable errors, as reported above such as in Figure 11.

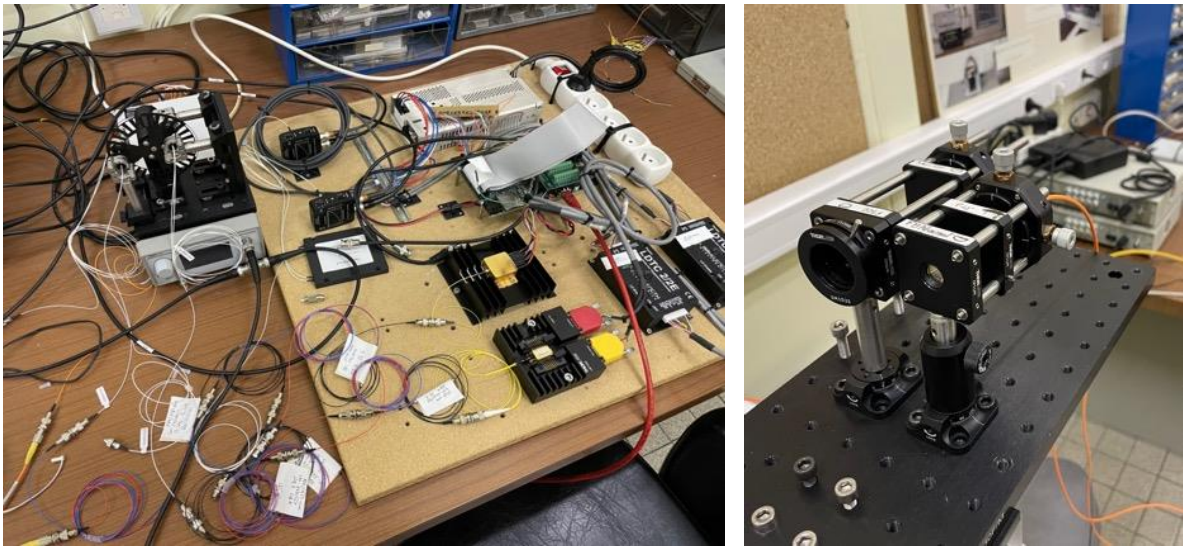

Figure 21. Next generation bi-color pyroreflectometer prototype used as base donator instrument to build a solarblind bi-color pyroreflectometer.
Left: core components (diodes, laser, DAQ, optical splitter, lock-in wheel…).
Right: optical head to measure light from sample and send reference lighting.

Therefore, bother theoretical and experimental investigations have been conducted based on a next generation bi-color pyroreflectometer prototype existing at PROMES-

CNRS in order to evaluate if other wavelengths could be usable in such a device to achieve solarblindness.

The recent prototype instrument used as donator notably relies on software lock-in signal isolation techniques and suitable high-speed high-resolution data acquisition system for the receiving diodes (pyrometer part) and the laser emission diodes (reflectometer part). Thanks to this feature, this instrument exhibit exceptional signal to noise ratio, allowing to use wavelengths with low photons count according to Wien's law and expected material behaviour at targeted temperature range: < 200 to >1000°C. Therefore, it was possible to investigate other wavelengths possibilities.

Two wavelengths were selected to upgrade this prototype in order to build a solarblind bi-color pyro-reflectometer: 1.87 µm and 2.7 µm. The optical components are commercially available at a reasonable price and exhibit suitable characteristics, including diodes, lasers, optical splitters, fiber optics… the key components (except the optical head with its fiber optics) have been gathered and assembled to upgrade the existing non-solarblind prototype to check its metrological performance in laboratory conditions: using PYROX calibrated blackblody up to 1600°C in air.

At this step, this solar blind bi-color pyro-reflectometer, based on high-speed software lock-in and working at 1.87 and 2.7 µm, exhibits promising performance in lab with a reference black body: it should allow measurement from 150-200°C to 1500+ °C for high absorptivity materials with lower uncertainty than the existing OPTRIS pyrometer.

In a next step, a dedicated optical head should be designed, built and tested on a solar facility to verify its actual performance on a setup such as the SAAF and verify if its added complexity is worth its improved measurement performance compared to a simple pyrometer and welded thermocouples.

2. Improvement of CIEMAT concentrated solar ageing services

A new test facility for accelerated aging testing of small cylindrical samples of solar receiver materials (Figure 22) have been developed and installed at the PSA Solar Furnace SF60 [13]. Realistic operating conditions are difficult to reproduce in laboratories, and central towers are not available for long term research purposes. Consequently, this facility aims to simplify the solar receiver aging analysis presenting a novel test bench that can measure the aging of a solar receiver under operating conditions typical of a central tower system. The aging will be measured by means of efficiency loss and mechanical damage as a function of temperature, concentrated solar flux and stress.

Figure 22. Novel test bench for accelerated aging testing of small cylindrical samples of solar receiver materials, built, developed and characterized at the PSA Solar Furnace SF60

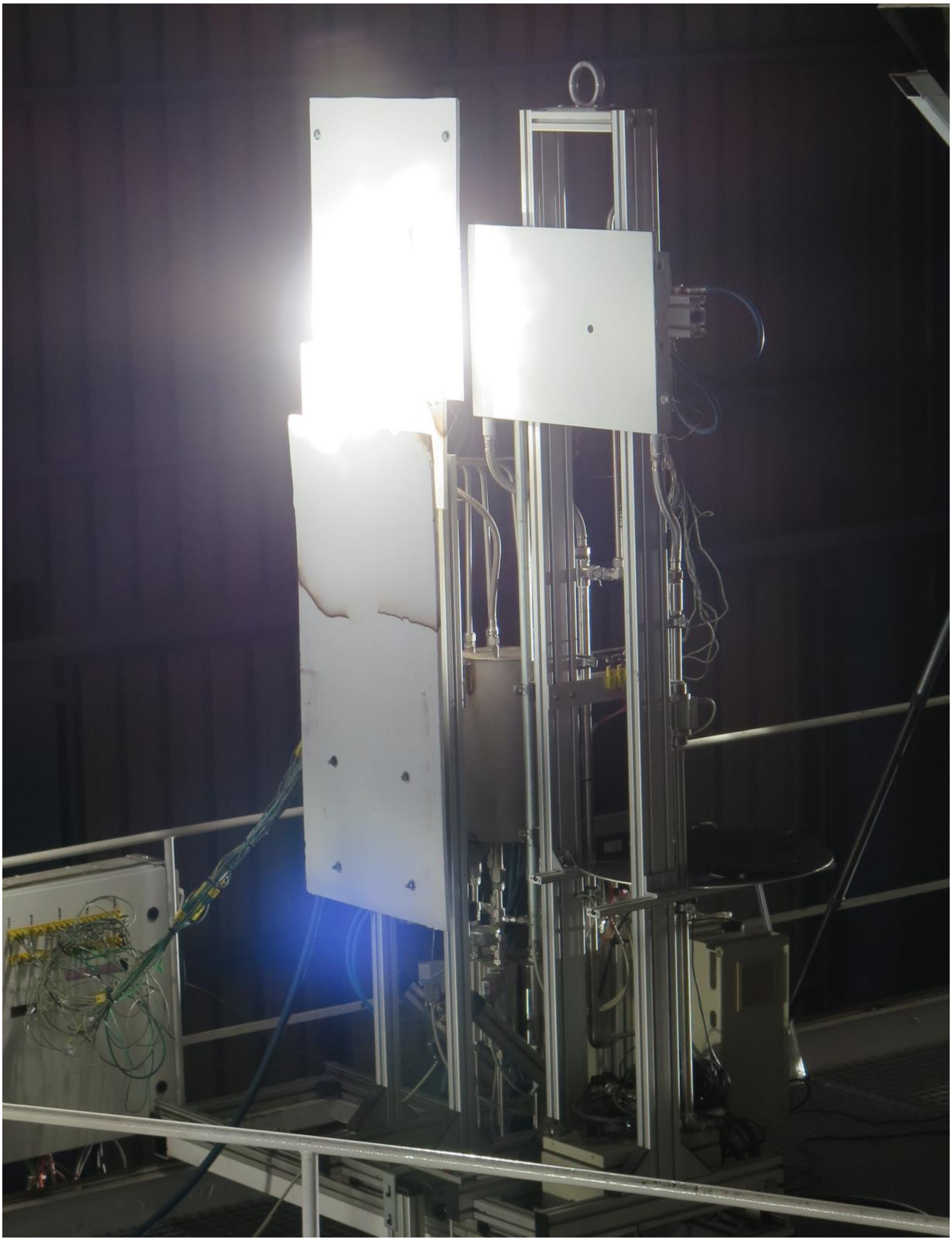

Figure 23. Close up on the Novel Solar Ageing test bench under solar ageing test.

This novel test bench for accelerated aging testing of small cylindrical samples [14] has been characterized with a tubular sample with a diameter of 1 inch and 1mm of thickness (Figure 24). It is made of 625 alloy and coated with Pyromark 2500, similar to tubes used in commercial solar receivers, but can be adapted to any other tubular sample. Solar radiation is concentrated on a tubular sample located at focus of the SF60. This solar furnace has the capability to tune the solar radiation to the required level of the test up to 3000 kW/m^2 by varying the shutter aperture.

Figure 24. Tubular sample for accelerated aging test

The tubular sample is cooled internally with a pressurized air stream up to 1,069 m^3 /min at 10 bar and ambient temperature. The low temperature and high flow rate of the air assure a cooling capacity similar to other more complex fluids like molten salts with a simpler setup. Figure 25 shows the test bench during its characterization campaign.

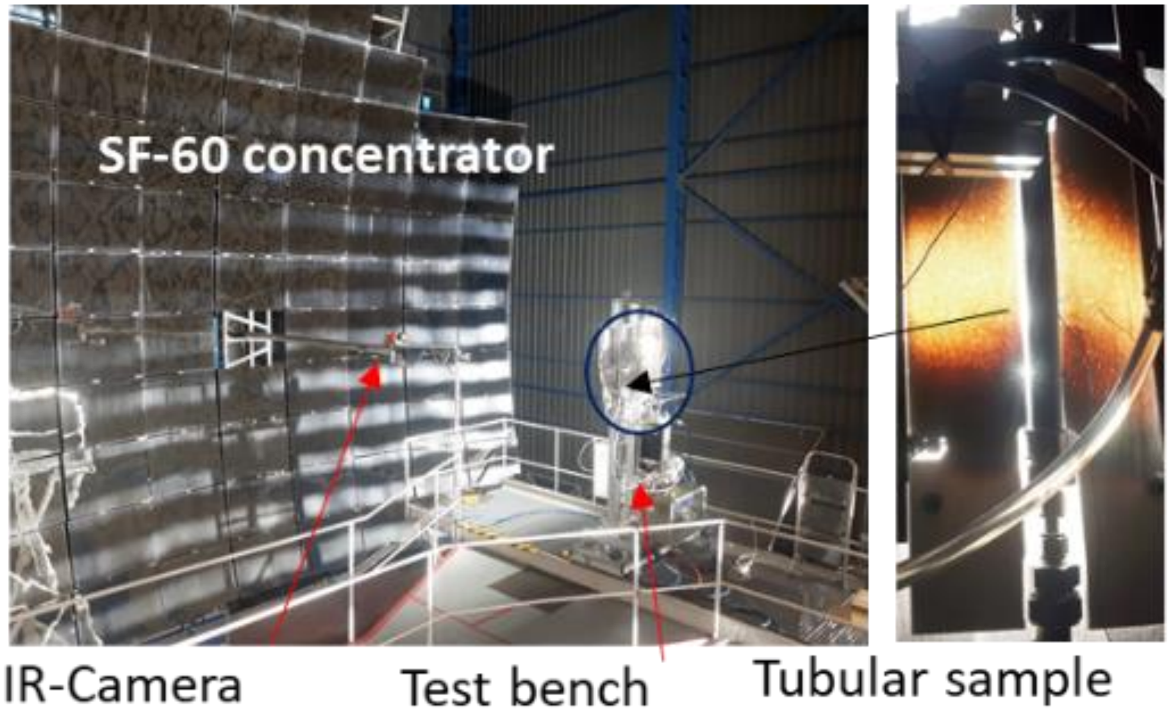

Figure 25. Novel test bench for tube type receivers aging during its characterization

The variables responsible for the receiver degradation (temperature, solar flux and stress) were measured as follows:

- Solar radiation on the receiver surface is measured using a Lambertian target (ProHERMES method [15], see Figure 26.a left);

- The radial and circumferential spatial distribution of metal temperature is measured with 5 thermocouples;

- the air inlet/outlet temperatures are also measured with thermocouples;

- the temperature distribution of the irradiated surface is measured with a solar blind infrared camera (see Figure 26.b left).

The temperature distribution is used to estimate the thermal stress by means of correlations available in the literature and to validate a FEM thermo-mechanical model of the tube samples tested. Figure 26.b shows a typical result obtained during the experimental test campaign.

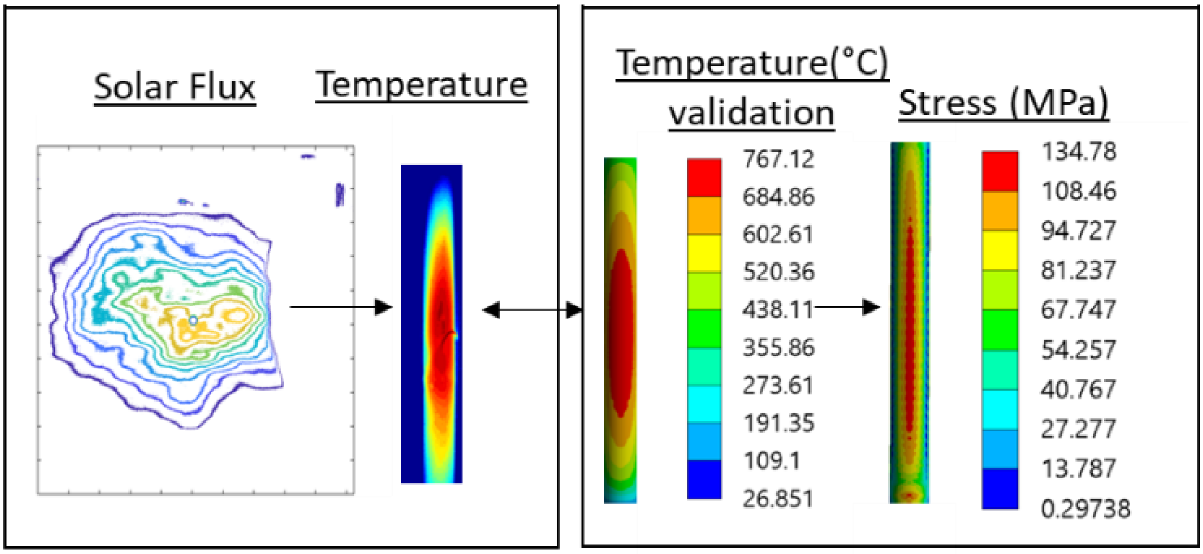

Figure 26. a) Typical solar flux and temperature spatial distribution on a tube. b) Typical stress spatial distribution calculated with a thermomechanical FEM model of the tube sample.

As results of a solar ageing test campaign (Figure 26), Figure 27 shows the aging condition map of the tube sample tested in the test bench, the maximum temperature value, as a function of temperature gradient across the irradiated wall (temperature difference internal-external tube wall) for different solar fluxes. As can be seen, the aging condition are in the range of solar tower receiver's operating conditions; temperatures between 500-850°C, solar fluxes up to 450 kW/m² and a temperature difference across the wall up to 90°C.

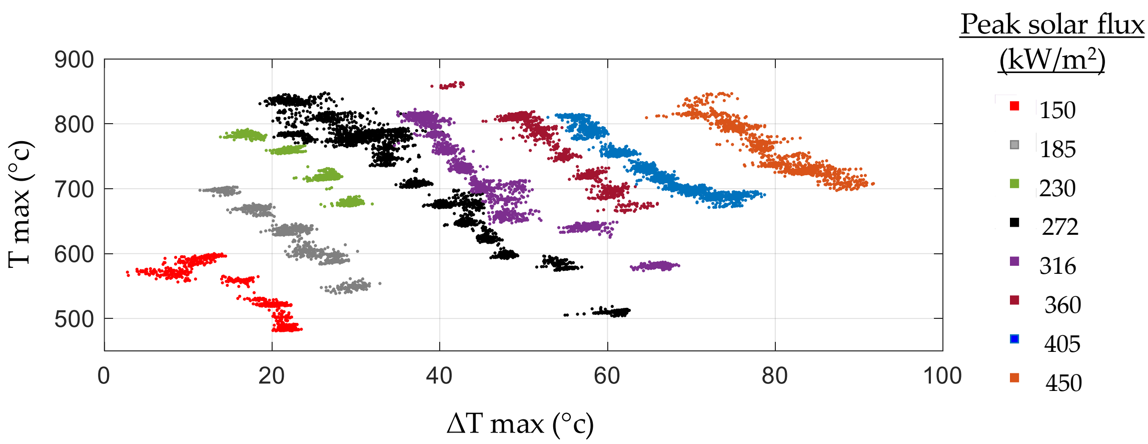

Figure 27. Aging condition map; maximum temperature of the tube sample as a function of temperature difference across the tube wall for different solar fluxes.

So, this new test bench can reproduce the long-term aging of solar receivers in realistic conditions similar to those of commercial solar plants. Moreover, this test bench allows to measuring the parameters relevant in the aging of receiver tubes (temperature, thermal stress, solar flux) and their impact on efficiency loss and mechanical failure. Thereby, this facility developed at CIEMAT-PSA can make easier to obtain very useful information for next commercial plants.

3. Conclusions

New developments for the Solar Accelerated Aging Facility were implemented at CNRS and at CIEMAT, to better adapt it to new requirements expressed by the users.

At PROMES-CNRS**, a new adaptable sample holder was designed**, fabricated and commissioned to allow for samples of various shapes (round, square, rectangular) and dimensions (typically 1” to 2” in size and 2 to 10 mm in thickness) to be tested while also enabling backside air cooling and thermocouple backside temperature measurement.

The validity of sample surface temperature measurements by IR pyrometry was assessed in the case of highly IR-reflective / low IR-emissive samples such as solar selective absorber coatings, which intrinsically provide low signal-to-noise ratio (the latter was quantified by calculations). Some recommendations can be made:

- for low temperatures (< 400°C), another potentially more suitable pyrometer was identified, although it may be less adapted for higher temperatures;
- thermocouple measurements can also be an alternative for the estimation of surface temperature, as there exists a linear correlation with the surface temperature measured by pyrometry. However, their implementation can be heavy if they are welded on the sample before each SAAF exposure. The touching thermocouple on the back center of the sample directly below the SAAF-irradiated area, integrated to the new sample holder, is a more repeatable and easier method of estimating the sample temperature with thermocouples;
- solar-blind pyroreflectometry could also be a good alternative for surface temperature measurement, as it does not require the knowledge of the sample spectral emittance and provides its true temperature.

At CIEMAT-PSA, a **new ageing test bench was developed** for solar receivers and tested with a tubular receiver mockup. The sample surface temperature measurements were provided by an IR solarblind camera in order to provide the temperature distribution on the sample receiver at the focal point of the solar furnace SF60. Together with PROHERMES flux measurements and a state-of-the-art FEM model of the receiver, **mechanical stresses** can be evaluated in the sample.

4. References

[1] A. Boubault, Etude du vieillissement de matériaux sous haut flux solaire concentré – Application aux récepteurs surfaciques des centrales solaires thermodynamiques, These en préparation, Perpignan, 2009. http://www.theses.fr/s83622 (accessed July 15, 2020).

[2] A. Boubault, B. Claudet, O. Faugeroux, G. Olalde, J.-J. Serra, A numerical thermal approach to study the accelerated aging of a solar absorber material, Solar Energy. 86 (2012) 3153–3167. DOI:10.1016/j.solener.2012.08.007.

[3] A. Boubault, B. Claudet, O. Faugeroux, G. Olalde, Accelerated Aging of a Solar Absorber Material Subjected to Highly Concentrated Solar Flux, Energy Procedia. 49 (2014) 1673–1681. DOI:10.1016/j.egypro.2014.03.176.

[4] A. Boubault, B. Claudet, O. Faugeroux, G. Olalde, Aging of solar absorber materials under highly concentrated solar fluxes, Solar Energy Materials and Solar Cells. 123 (2014) 211–219. DOI:10.1016/j.solmat.2014.01.010.

[5] D. Hernandez, G. Olalde, J.M. Gineste, C. Gueymard, Analysis and Experimental Results of Solar-Blind Temperature Measurements in Solar Furnaces, J. Sol. Energy Eng. 126 (2004) 645–653. DOI:10.1115/1.1636191.

[6] K. Niranjan, P. Kondaiah, G. Srinivas, H.C. Barshilia, Optimization of W/WAlSiN/SiON/SiO2 tandem absorber consisting of double layer anti-reflection coating with broadband absorption in the solar spectrum region, Applied Surface Science. 496 (2019) 143651. DOI:10.1016/j.apsusc.2019.143651.

[7] A. Dan, J. Jyothi, K. Chattopadhyay, H.C. Barshilia, B. Basu, Spectrally selective absorber coating of WAlN/WAlON/Al2O3 for solar thermal applications, Solar Energy Materials and Solar Cells. 157 (2016) 716–726. DOI:10.1016/j.solmat.2016.07.018.

[8] A.D. Rakić, A.B. Djurišić, J.M. Elazar, M.L. Majewski, Optical properties of metallic films for vertical-cavity optoelectronic devices, Appl. Opt., AO. 37 (1998) 5271–5283. DOI:10.1364/AO.37.005271.

[9] Sh.A. Furman, A.V. Tikhonravov, Basics of optics of multilayer systems, Editions Frontières, Gif-sur-Yvette, France, France, 1992.

[10] A. Carling Plaza, Vieillissement accéléré et durabilité de matériaux sélectifs pour récepteurs de centrales solaires à concentration, These de doctorat, Perpignan, 2021. http://theses.fr/s237867 (accessed December 18, 2021).

[11] D. Hernandez, J.M. Badie, F. Escourbiac, R. Reichle. Development of two-colour pyroreflectometry technique for temperature monitoring of tungsten plasma facing components. Fusion Engineering and Design, Volume 83, Issue 4, 2008,Pages 672-679, DOI: 10.1016/j.fusengdes.2008.02.008

[12] Hernandez, D., Sans, J. L., and Pfänder, M. (June 13, 2008). Pyroreflectometry to Determine the True Temperature and Optical Properties of Surfaces. ASME. *J. Sol.*

Energy Eng. August 2008; 130(3): 031003. DOI: 10.1115/1.2840575

[13] PSA SF60 solar furnace renewed. Rodríguez, J.; Cañadas, I.; Monterreal, R.; Enrique, R. and Galindo July 2019. AIP Conference Proceedings 2126(1):030046. DOI: 10.1063/1.5117558

[14] Building a test bench to predict the reliability of solar receiver. E. Setién, J. Garrido, S. Caron, L. Valenzuela, J. Fernández-Reche). SolarPaces Proceedings. October 1-4, 2019, Daegu (South Korea).

[15] CCD flux measurement system PROHERMES. A. Kröger-Vodde and A. Holländer. Proceedings of the 9th SolarPACES International Symposium on Solar Thermal Concentrating Technologies. DOI: 10.1051/jp4:19993103

5. Annexes

Annex 1. CNRS SAAF pyrometer calibration data

Table 3. **Temperature read by the pyrometer with input emittance of 0.98 vs. real temperature of detected blackbody.**

SR-2 blackbody ***T*** **(°C)** ***ε = 0.99 ± 0.01***	**Pyrometer** ***T*** **(°C)** **ε = 0.98**	**Absolute error with pyrometer (°C)**	**Relative error with pyrometer (%)**
250	256.3	+6.3	+2.5%
300	294.8	-5.2	-1.7%
350	342.6	-7.4	-2.1%
400	389.4	-10.6	-2.7%
450	439.0	-11	-2.4%
500	487.9	-12.1	-2.4%
550	537.2	-12.8	-2.3%
600	586.3	-13.7	-2.3%
650	637.0	-13	-2.0%
700	686.8	-13.2	-1.9%
750	737.0	-13	-1.7%
800	787.5	-12.5	-1.6%
850	838.9	-11.1	-1.3%
900	889.7	-10.3	-1.1%
950	940.5	-9.5	-1.0%
1000	992.7	-7.3	-0.7%
1050	1044.0	-6	-0.6%
1100	1097.0	-3	-0.3%
1150	1149.0	-1	-0.1%

Annex 2. Characteristics of OPTRIS pyrometers

This data was retrieved on OPTRIS websites (www.optris.co.uk / www.optris.fr).

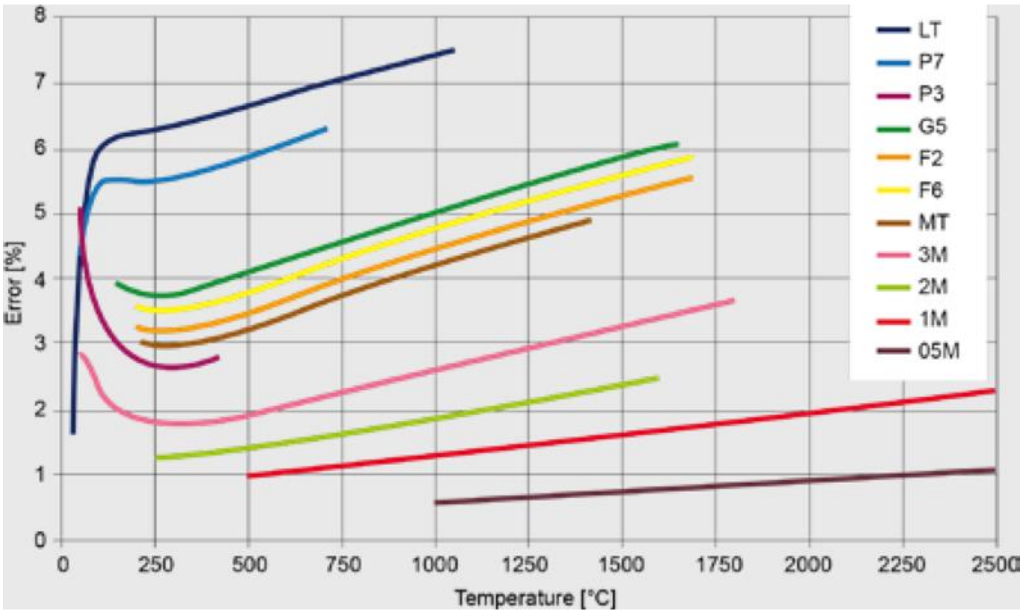

Figure 28. Measurement errors across different wavelengths if the emissivity is wrongly adjusted by 10%

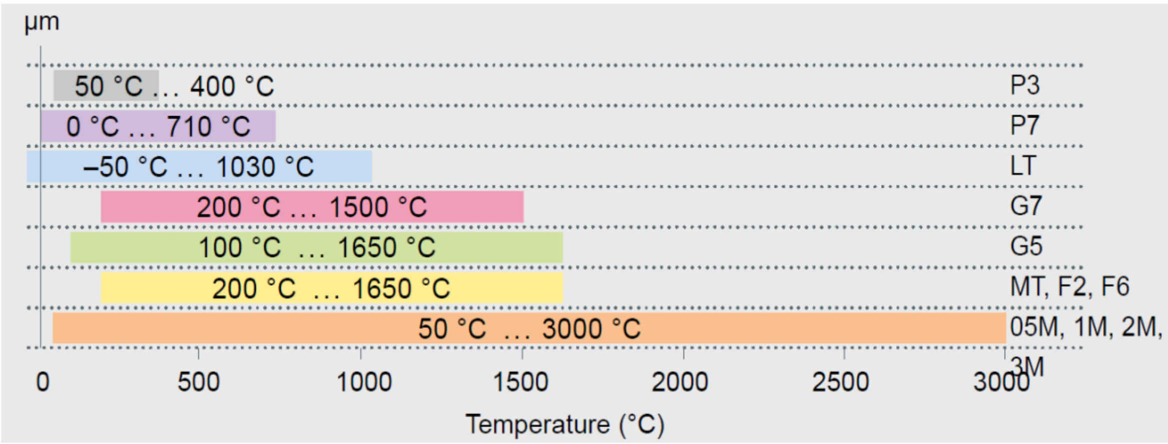

Figure 29. Temperature range of OPTRIS pyrometers

- 8 – 14 µm for non-metal surfaces (Type of device: LT)
- 0.5; 1.0; 1.6; 2.3 µm mainly for liquid metals and metal surfaces (Type of device: 05M; 1M; 2M; 3M)
- 3.43 µm for thin plastic films like PE, PP and PS (Type of device: P3)
- 3.9; 4.24; 4.64; 7.9 µm for special applications (Type of device: MT; F2; F6)
- 5.0 µm for glass surfaces (Type of device: G5)
- 7.9 µm for plastic foils and glass surfaces (Type of device: P7/G7)

Figure 30. Wavelength ranges of OPTRIS pyrometers